Movement mechanism of boulders composing valley bank and beds by debris flows and development of debris flow front using the APM method

Hiroki Kato[1*], Shoji Fukuoka[2]
[1]Civil, Human and Environmental Engineering, Chuo University, 1-13-27 Kasuga, Bunkyo-ku, Tokyo 112-8551, Japan
[2] Research and Development Initiative, Chuo University, 1-13-27 Kasuga, Bunkyo-ku, Tokyo 112-8551, Japan.
* Corresponding author. Tel.: +81 3 3817-1615. E-mail address: a17.jnt5@g.chuo-u.ac.jp.

keyword : *debris flow, valley bank and bed erosion, the one-fluid model of solid-liquid multiphase, APM method*

1. Introduction

Clarifying the erosion mechanism of a valley by a debris flow is important not only for evaluating the amount of debris flow that passes through the valley, but also for evaluating the stability of the valley beds and banks after the debris flow has passed. However, the erosion mechanism of valley beds and banks by debris flows has not been fully clarified.

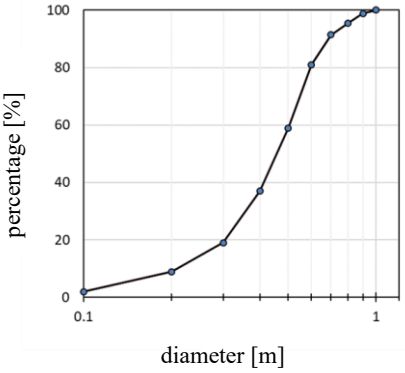

Fig. 1 Particle size distribution

Iverson et al. [1] measured the total stress and pore water pressure acting on the channel bed during debris flow passage using large scale model experiments, and showed that the momentum of the debris flow is increased by entrainment due to liquefaction of the channel bed. Lyu et al. [2] focused on bank erosion caused by the passage of debris flow and compared the flow and erosion between cases where bank erosion is dominant and cases where only bed erosion occurs. The results show that valley bank erosion contributes more to the growth of the debris flow front than bed erosion, and that valley bank erosion occurs after the front of debris flow has passed.

However, it is difficult to measure the forces acting on individual particles and the flow field around the particles in these model experiments, which can only be done by numerical analysis. Euler-Euler type approach is less computationally demanding than the Euler-Lagrange type approach and analyzes in the field scale. But it does not elucidate the essential phenomena of the debris flow. In recent years, with the improvement of computer performance, the Euler-Lagrange type model has been developed. Fukuda et al. [3] developed the Euler-Lagrange type model (APM method) that can analyze non-spherical particles, and explained the results of the debris flow channel experiment conducted by Ito et al.

In this study, as basic research on the erosion mechanism of valley bank and bed, a straight valley shape with mobile valley bed and bank is created. The results of the numerical experiment are compared with the results of the model experiment and the factors causing the movement of individual particles are discussed.

2. Numerical methods

2.1. Numerical method of fluid motions

In the flow analysis with the stone and gravel particles, a one-fluid model of solid-liquid multiphase flow is used, where the solid phase is given as a fluid with different densities, and the whole is assumed to be an incompressible fluid. The basic equation of the flow is shown below.

$$\frac{\partial u_i}{\partial x_i} = 0 \tag{1}$$

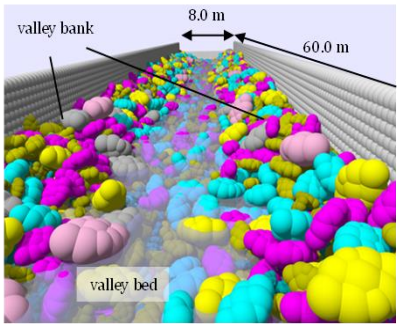

Fig. 2 Initial state

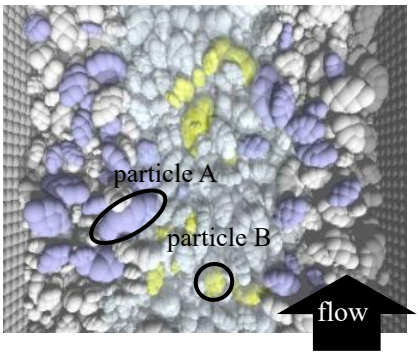

Fig. 3 State of before the passage of the debris flow front

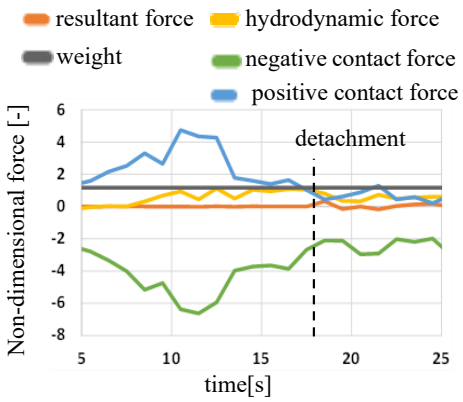

(a) Particle A

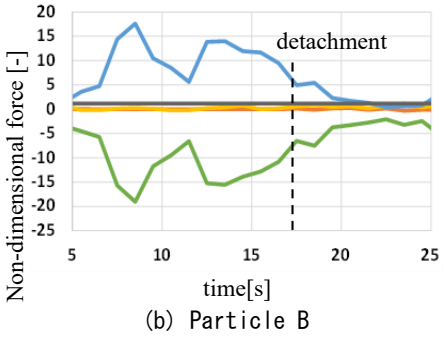

(b) Particle B

Fig. 4 Time variation of the longitudinal non-dimensional force

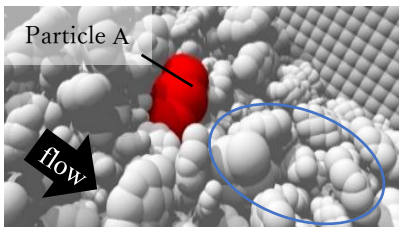

(a) Just before the arrival of the debris flow front

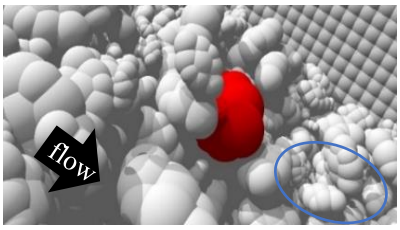

(b) Just before particle A starts to move

Fig. 5 stone and gravel around particle A

$$\frac{\partial u_i}{\partial t} + u_j \frac{\partial u_i}{\partial x_j} = g_i - \frac{1}{\rho}\frac{\partial P}{\partial x_i} + \frac{\partial}{\partial x_j}\{2(\nu + \nu_t)S_{ij}\} \tag{2}$$

$$\nu_t = (C_s\Delta)^2\sqrt{2S_{ij}S_{ij}} \tag{3}$$

where ρ and u_i are the volume average density and the mass average velocity, respectively, taking into account the volume fraction of the particles in a computation grid. ν is the kinematic viscosity, g_i is the gravitational acceleration, P is the sum of the isotropic components of pressure and SGS stress, S_{ij} is the strain rate tensor, ν_t is the turbulent viscosity, and C_s is the Smagolinsky constant. Δ is the computation grid size. The free water surface was simulated using the volume of fluid (VOF) method.

2.2. Numerical method of gravel motions

The motion of the particles is solved using the equation of motion of a rigid body, and the contact judgment and contact force of the gravels are evaluated using the distinct element method for each gravel particle. The hydrodynamic forces on the particles are calculated directly by volume integration of the pressure and diffusion terms in the equation of motion of the flow field. The basic equations are shown below.

$$M\ddot{r}_i = Mg_i + F_i^f + F_i^c \tag{4}$$

$$\dot{\omega}_{i'} = I_{i'j'}^{-1}\{R_{j'i}(T_i^f + T_i^c) - \varepsilon_{j'k'l'}\omega_{k'}I_{l'm'}\omega_{m'}\} \tag{5}$$

where, where the index i denotes the components of the global coordinate system fixed on the space, the indices i'–m' denote the components of the local coordinate system fixed on a rigid body, M is the mass of a particle, r_i^g is the position of the center of gravity of the rigid body, ω_i is the angular velocity, F_i is the force acting on the surface of the particle, and T_i is the torque on the center of the gravity generated by the force. The superscripts f and c are the components of the fluid forces and contact forces between particles, respectively, g_i is the gravitational acceleration, $I_{i'j'}^{-1}$ is the inverse of the matrix consisting of the components of the moment of inertia tensor in the local coordinate system, $R_{j'i}$ is equal to $\boldsymbol{e}_{j'} \cdot \boldsymbol{e}_i$ ($\boldsymbol{e}_{j'}$ and $\boldsymbol{e}_i$ are unit basis vectors), and $\varepsilon_{j'k'l'}$ is the Levi–Civita symbol.

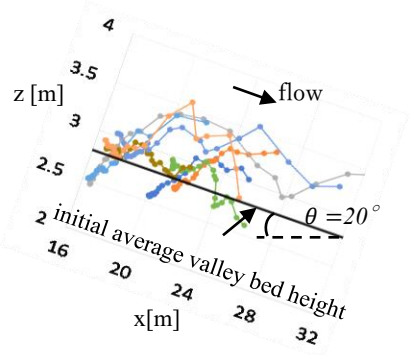

(a) Particle with a diameter of more than 0.5m

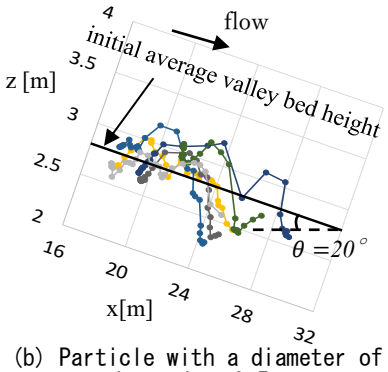

(b) Particle with a diameter of less than 0.5m

Fig.6 Position of the center of gravity for each of the particles

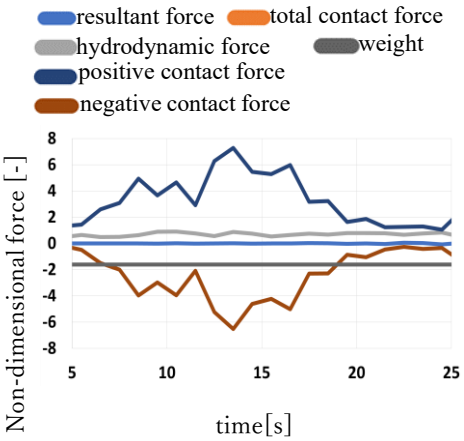

Fig.7 Time variation of the non-dimensional vertical force acting on particle B

3. Experimental conditions of the numerical movable-bed channel

The numerical movable-bed channel used in this study is a straight channel of 60 m in length and 8 m in width. The slope of the channel was set to 20°. The coordinate axes are the x-axis in the downstream direction, the y-axis in the transverse direction, and the z-axis in the upward direction (the z-axis direction is referred to as the vertical direction). We used non-spherical particles of the valley bed and bank consisting of 10 different particle sizes, with the largest particle size being 1.0 m and the smallest being 0.1 m, as shown in Figure 1. All the particles are equal in shape and density. The diameters of non-spherical particles were defined as the diameters of spheres with the same volume.The particles were randomly dropped into the channel, and the initial channel form was set up with the slope of the valley bank at about 30 degrees and is shown in Figure 2. In the experiment, a constant flow rate of 10.0 $[m^3/s]$ was continuously applied at the upstream end of the channel. No sediment was supplied to the flowing water. At the downstream end, the pressure was set to zero and the sediment was discharged out freely. The debris flow front was formed by taking particles from the valley bed and bank.

4. Movement mechanism of valley bank and bed particles

We focused on particles that had moved more than 5 meters in the longitudinal direction from the section where the debris flow front had passed. In Figure 3, the blue particles are the valley bank particles and the yellow particles are the valley bed particles. The number of valley bank particles and bed particles we focused on was 38 and 14, respectively.

4.1. Movement mechanism, of valley bank particles

The main force causing the movement of 38 sample particles of the valley bank was as follows: 1 particle was due to hydrodynamic forces, 5 due to collision forces, 23 due to a decrease in resistance force, and 9 due to other factors. The decrease in the resistance force implies the decrease in the contact force and brought the start of the longitudinal movement of the valley bank particles. Figure 4 demonstrates time variations of the longitudinal force acting on particles A and B shown in Figure 3. The positive contact force and fluid force on particle A in Figure 4(a) increase with the arrival of the debris flow front. However, the negative contact force also increases, and the resultant force becomes zero and the particle does not start to move. At about 18 seconds after the arrival of the debris flow front, particle A starts to move, although the force is smaller than when the debris flow front arrived. Figure 5 shows the state of the gravel around particle A just before the arrival of the debris flow front and just before the start of movement. The red particle is particle A. Figure 5 shows that just before the arrival of the debris flow front, the particles on the downstream side of the debris flow are firmly interlocked, taking placement where they can produce a large resistance force. On the other hand, just before particle A starts to move, the surrounding stones and gravels break down their alignment. Particularly, the particles on the downstream side have been shifted, and particle interlocking has taken worse alignment. It is thought that the resistance force of the site is smaller than that before the arrival of the debris flow front, and this causes the valley bank particles to start moving and the scale of debris flow front to grow.

4.2. Movement mechanism, of valley bed particles

The movement of particles that make up the valley bed were analyzed in the same way as that of the particles that form the valley bank. The 14 specimens were examined. The main factor that caused the particles to start moving in the longitudinal direction was hydrodynamic force (2 specimens), collision (1 specimen), reduced resistance (11 specimens), and other factors (0 specimens). The main factor in the movement of the particles that make up the valley bed is a decrease in the resistance force. Figure 4(b) shows that, when the debris flow front reaches particle B, both the hydrodynamic force and the positive contact force increase, and the negative contact force also increases, like particle A, so the resultant force is zero and the particle does not start moving. After that, the particle started to move with less force than when the debris flow front arrived.

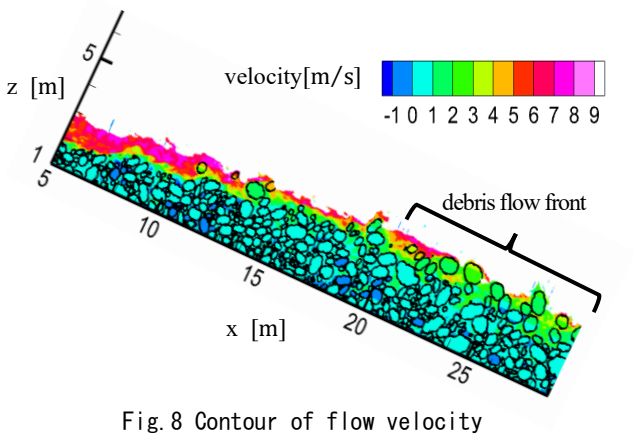

Fig. 8 Contour of flow velocity

Figure 6 shows change in the position of the center of gravity for each of the particles of interest in the valley bed. Figure 6 shows that the particles on the surface of the valley bed first move vertically upward, and then begin to move longitudinally. It is thought that the particles of the valley bed begin to move because they decrease contact force in the negative direction by moving vertically upward. In addition, for particles in the valley bed, the smaller particles moved to a lower position in relation to the initial valley bed. It is thought that the smaller particles drop among the larger particles.

The particles on the valley bed surface began to move at about 18.6 seconds. This is the time when the rearmost part of the debris flow front is passing through the location of the particles of interest. In other words, the particles on the surface of the valley bed begin to move not when the debris flow front arrives and exerts a large force, but when the debris flow front passes by.

Figure 7 shows the time variation of the non-dimensional vertical force acting on particle B. The absolute value of the contact force in the negative direction increases with the arrival of the debris flow front. It is thought that the force is exerted to the vertical downward direction from the particles constituting the debris flow front, which acts as a resistance force and prevents the particles from starting to move.

Figure 8 shows the velocity contour map during the passage of the debris flow front. It is seen that the velocity of the debris flow front is small, while the velocity of the following flow is large. This is similar to the experimental results of Lyu et al. [2]. Unstable gravel and stone particles on the bed of the channel after the debris flow front passed through are supplied into the front of debris flow by the fast flow of the following stream.

5. Conclusion

In this study, the erosion mechanisms of individual particles in a valley were investigated using the APM method. The results of numerical experiments were similar to those of previous experimental studies. The particles on the bank and bed of the valley are eroded due to a decrease in resistance force. Valley bank particles had reduced resistance due to the discharge of downstream particles, and valley bed particles had reduced resistance due to moving to a relatively higher position than the surrounding particles. It is clear that particles initiating migration by such a mechanism is transported to the debris flow front by the following flow and that a debris flow develops.

References

[1] Richard M. Iverson, Mark E. Reid, Matthew Logan, Richard G. LaHusen, Jonathan W. Godt and Julia P. Griswold: Positive feedback and momentum growth during debris-flow entrainment of wet bed sediment, Nature Geoscience, Volume 4, pp.116-121, 2011

[2] Richard M. Iverson, Mark E. Reid, Matthew Logan, Richard G. LaHusen, Jonathan W. Godt and Julia P. Griswold: Positive feedback and momentum growth during debris-flow entrainment of wet bed sediment, Nature Geoscience, Volume 4, pp.116-121, 2011

[3] Fukuoka, S., Fukuda, T., Uchida, T., 2014. Effects of sizes and shapes of gravel particles on sediment transports and bed variations in a numerical movable-bed channel, *Adv. in Water Res.*, 72, 84-96, https://doi.org/10.1016/j.advwatres.2014.05.013.